Optics Letters

Measurement of the $5S_{1/2}$ to $5D_{5/2}$ two-photon clock transition frequency of rubidium-85 in high vacuum

Chi-Hsiang Chu,[1] Po-Cheng Chang,[2] Yu-Jhe Shih,[1] Dah-An Luh,[1,3] Ming-Shien Chang,[4] Tze-Wei Liu,[5] Yi-Ting Lin,[1] Bo-Wei Chen,[1] and Wang-Yau Cheng[1,6,*]

[1]Department of Physics, National Central University, Taoyuan City 32001, Taiwan
[2]Advanced Technology Laboratory, Chunghwa Telecom Laboratories, Taoyuan City 32661, Taiwan
[3]National Synchrotron Radiation Research Center, Hsinchu 30076, Taiwan
[4]Institute of Atomic and Molecular Science, Academia Sinica, Taipei 11529, Taiwan
[5]Hon Hai Research Institute, Taipei 11492, Taiwan
[6]Quantum Technology Center, National Central University, Taoyuan City 32001, Taiwan
*Wycheng@phys.ncu.edu.tw

Received 29 September 2023; accepted 19 October 2023; posted 23 October 2023; published 9 November 2023

We present a scheme to precisely resolve the unperturbed line shape of an optical rubidium clock transition in a high vacuum, by which we avoided the systematic errors of "collision shift" and "modulation shift." The spectral resolution resolved by this scheme is significantly improved such that we can use "Zeeman broadening" to inspect the stray magnetic field, through which we were able to compensate the magnetic field inside the Rb cells to be below 10^{-3} Gauss. We thus update the absolute frequency of the clock transition and propose a standard operation procedure (SOP) for the clock self-calibration.

https://doi.org/10.1364/OL.507165

The optical rubidium clock (Rb_{opt} clock) at 778-nm wavelength is one of the most popular secondary optical clocks owing to its excellent frequency stability [1] and the feasibility in terms of portability [2–4] and miniaturization [5]. Moreover, it becomes an important frequency standard in telecommunication [6] since the related 1556-nm fundamental wavelength is within the ITU C-band DWDM grid. In our laboratory, the Rb_{opt} clock is an important frequency reference to our Ti:sapphire (Ti:S) comb laser [7]. However, sources of errors need to be clarified and mitigated before an Rb two-photon stabilized laser is used as a frequency standard. For instance, the permeation of helium from the ambient air to glass cells was recently proved to cause collisional frequency shift and broadening in glass cell-based frequency standards [8]. Another example is the "modulation shift and broadening" [9,10]. In this paper, the aforementioned two systematic errors are avoided, and the Zeeman shift is reduced to be below our measurement precision.

The flowcharts in Fig. 1 are used to illustrate our scenario in which the second harmonic (SH) of a commercial 1556-nm fiber laser [11] was used as the light source, in which the power in 778 nm was 200 mW, with a well-collimated 0.6-mm beam diameter, measured by the "knife-edge" approach [12]. The double-pass AOM is for regulating laser power and for the fast feedback to reduce laser jitter from the original 2-MHz jitter width down to 70-kHz width, via a Pound–Drever–Hall (PDH) scheme. That is, we have prepared a 778-nm light source having 70-kHz linewidth and 120 mW ± 20 μW power regulation where the laser frequency always follows the resonant frequency of one Fabry–Perot (FP, finesse ∼1000) cavity illustrated in Fig. 1. One portion of the laser power after AOM was sent to the EOM1-based Rb spectrometer to stabilize the frequency of the −1 sideband. The sideband was constantly dithered to stabilize its frequency to ^{87}Rb $5S_{1/2}$ ($F_g = 2$)→$5D_{5/2}$ ($F_e = 4$) two-photon transition. The principle and the detailed setup are the same as what has been reported in our previous works [10,13] except that the laser power is different. An 8.8-mW laser power was conducted to pass through the EOM1 and was aligned to overlap with the unmodulated counter-propagating beam (9.3 mW). Those two well-overlapped beams were focused into a rubidium cell (Rb cell #1) by a pair of lenses, resulting in a smaller laser beam diameter of 0.07 mm in the center of Rb cell #1. The EOM1 frequency Δ_0 is 1.152 GHz for bridging the isotope frequency between ^{87}Rb and ^{85}Rb. We dither the sidebands at a 27.7-kHz (ω_d) dither width with a 1.8-MHz FM amplitude (2A), that is, the modulation frequency of EOM1 is $\Delta_0 + A\cos\omega_d t$. The PMT1 in Fig. 1(a) is for detecting the 422-nm fluorescence from a level decay of 6P to ground state (5S) transition [1]. The lock-in amplifier (LA) output was fed back to PZT2 via a loop filter (LF) for laser frequency stabilization. On the contrary, if scanning laser frequency was demanded, the LA output would be connected to "B" and, meanwhile, the PZT2 be connected to "D" such that its length be scanned by a tooth voltage. The output of LA was sent to the upper channel of an oscilloscope shown in Fig. 1(b), red trace. The current amplifier (CA) output was simultaneously recorded at the lower channel of Fig. 1(b), black trace, where the abscissa of the data plot was calibrated by a Ti:S comb laser. The derivative-like "crossover" signal [10] on the red trace resulted from the two-photon resonant condition formed by one carrier photon and one sideband photon, whereas no "two-carrier-photons" transition was found in the red trace since the carrier frequency ω_c was not dithered. The lower channel of Fig. 1(b) demonstrates the discrepancy between perturbed and unperturbed absorption spectra, showing that modulation broadening (perturbed) is inevitable [14] and thus is not appropriate

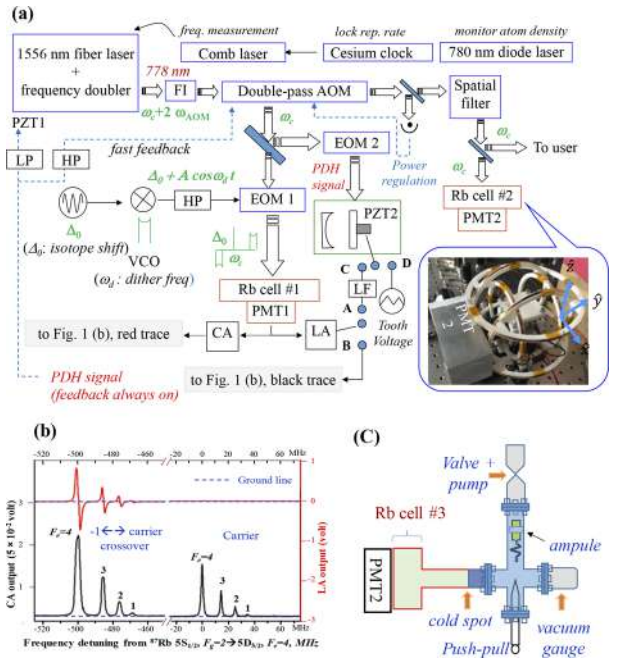

Fig. 1. (a) Schematic of our Rb clock system. FI, Faraday isolator; LA, lock-in amplifier, 30 ms time constant; CA, current preamplifier, 10-Hz low-pass filter; Δ_0, EOM1 freq.; LF, loop filter; HP, high-pass filter; LP, low-pass filter; PDH, Pound–Drever–Hall scheme. (b) Red trace, LA output for laser locking; black trace, CA output. (c) Structure of Rb cell #3 (see text).

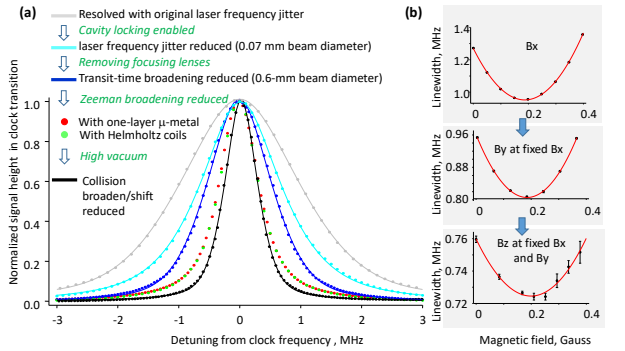

Fig. 2. Importance of the line shape analysis: (a) Normalized line shapes of clock transition under different conditions. (b) Analyzing the spectral linewidth versus magnetic field successively in three directions: *x*, *y*, and *z* directions are defined in Fig. 1(a).

for spectral line shape analysis. When the EOM1 −1 sideband was locked to the zero crossing of the derivative-like signal in Fig. 1(b), we started to scan the EOM1 frequency Δ_0 by which the ω_c is changed to resolve the ^{85}Rb $6D_{5/2}$ hyperfine spectra via either Rb cell #2 or cell #3. The Rb cell #2 in Fig. 1(a) was later replaced by the Rb cell #3 shown in Fig. 1(c) under the situations that the Helmholtz coils and PMT2 remained untouched since we only inserted the glass part (green color) of Rb cell #3 into the original location of Rb cell #2. The laser beam diameter in the center of Rb cell #2/#3 could be changed to be either 0.07 or 0.6 mm with or without additional focusing lenses. Rb cells #1 and #2 are commercial glass cells, whereas Rb cell #3 was home-designed including a glass cell (green color) connected to a stainless chamber (purple color), a cold-cathode gauge, and a pig-tailed rubidium ampule. The ampoule was held by stainless steel foils spot-welded onto the interior wall of the chamber. A pumping station was used to pump the entire system to be below 3×10^{-7} Torr. After the vacuum system was sealed with a gate valve, the pigtail of the ampule was smashed with a push–pull linear feedthrough, and the rubidium atoms were then diffused out. Rubidium atoms were collected gradually to a certain place, which is named the "cold spot" in Fig. 1(c). During the data acquisition period, the temperature of the ampule and the three windows of Rb cell #3 were always kept much higher than the cold-spot temperature. That is, the windows for the passages of laser beams and fluorescence in Fig. 1(c) were kept at a temperature of around 90°C, while the cold-spot temperature was kept at 52°C in most experimental situations. After the cold spot gathered enough condensed atoms, the gate valve was re-opened, while the vacuum pump was kept working until all data acquisitions were finished. Two approaches of keeping away the influence of Earth's magnetic field are used: Rb cell #1/#2 was wrapped with one-layer μ-metal, while three pairs of Helmholtz coils were applied onto Rb cell #2/#3. A 780-nm diode laser was used to probe Rb D2 transition as the peak height of the Doppler-broadened absorption signal is proportional to the atom density.

Our scheme benefits for high-precision line shape analysis and the linewidth was found to be sensitive to the environmental situations. Taking Fig. 2(a) as an example, the broadened gray line implied a severe laser jitter. And indeed, we identified that the jitter was caused by the vibration of the fan blades inside the fiber laser system. A FP cavity was then used to reduce the frequency jitter. All the spectra in Fig. 2(a) were recorded with the clock transition (^{85}Rb $5S_{1/2}$, $(F_g = 3)\rightarrow 5D_{5/2}$ $(F_e = 5)$), and all the data were taken from Rb cell #2 except that the black dots were taken from Rb cell #3 for comparison. The narrowest linewidth of 510 (4) kHz (full width half maximum, FWHF), shown by the black line shape, implies that there exists some alien-gas collision in Rb cell #2 (723 kHz, FWHM). Since molecular collisions induce both spectral broadening and shift [8,15,16], the transition frequency determined by the narrowest linewidth in Fig. 2 is considered to be closest to the absolute transition frequency according to Refs. [8,16]. The green and red dots in Fig. 2(a) overlap together within our measurement uncertainty, regardless of the approaches we employed to keep away the Earth's magnetic fields. Figure 2(b) demonstrates the process of reducing the Zeeman broadening (via Rb cell #2), which is another example showing the advantage of our scheme. And with that, we can compensate the stray magnetic field (mainly from the Earth) by reducing the Zeeman broadening, which offers a unique approach to some places where the Gauss meter can't reach, such as the interior of an atom container. The mutual perpendicular "*x*," "*y*," and "*z*" directions in Fig. 2(b) are defined and indicated in Fig. 1 where the "*x*" axis is along the direction of light propagation. We first chose to change the "*x*" direct magnetic field (B_x) to search the narrowest linewidth with a polynomial function, and we found that a quadratic function could fit the data well as exhibited in Fig. 2(b). Once we can fix the "*x*" direction current at the narrowest linewidth, the next step will be to explore the other minimum linewidth currents in the same way in "*y*" and "*z*" direction until the narrowest linewidth currents of all three dimensions were confirmed, by which a 723 (5)-kHz (FWHM) linewidth was achieved with Rb cell #2. A similar operation procedure was also applied to Rb cell #3, and a 510 (4)-kHz minimum linewidth was obtained. We removed

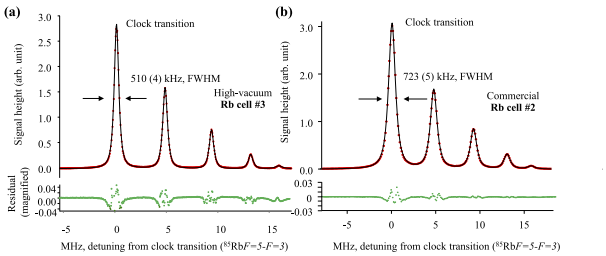

Fig. 3. Spectrum comparison (cells #1 and #2 have similar spectra), showing cell contamination in (b).

Table 1. Measured Clock Frequencies[a] and the Comparisons with CIPM Recommended Values

Upper State ($F_g = 3$)	[a]Abs. Freq. via Cell #2 (kHz)	[a]Abs. Freq. via Cell #3[b] (kHz)	[a]CIPM [14] (kHz)	Discrepancy from CIPM $\Delta f_{\#2}$	$\Delta f_{\#3}$
[c]$F_e = 5$	**42340.5 (2.3)**	**42369.2 (5.0)**	**42375 (5)**	**–34.5**	**–5.8**
$F_e = 4$	47064.9 (3.5)	47092.9 (2.8)	47093 (9)	–28.1	–0.1
$F_e = 3$	51568.2 (3.1)	51597.9. (2.5)	51603 (9)	–34.8	–5.1
$F_e = 2$	55375.4 (4.9)	55401.5 (2.1)	55406 (9)	–30.6	–4.5
$F_e = 1$	58101.8 (2.2)	58136.6 (6.3)	58146 (14)	–44.2	–9.4

[a] + 385285100000.0 kHz, extrapolating to 90°C Rb saturation vapor pressure from our 5.3 μTorr Rb pressure (see text).

[b]Vacuum cell

[c]Clock transition

Table 2. Error Budget, kHz (Clock Transition)

Statistic Error	Extrapolation to 90°C	Light Shift	Rb Self-collision	Cs Clock	Line Pulling
1.8	1.4	0.6	0.4	0.2	0.2

the Rb cell and inspected the residual magnetic field with our best Gauss meter on hand, and we found that the Earth's magnetic field had been reduced to be smaller than 1 mG, limited by our meter precision. Figure 3 compares the spectra resolved by the Rb cell #2 and Rb cell #3, from which we found not only collision broadening/shift in cell #2 but also a tiny "line pulling" effect by the neighborhood lines, as there is a 1.7-kHz discrepancy in clock transition between single-spectrum fitting and global fitting, whereas only 0.2-kHz discrepancy was found from the spectra of Fig. 3(a). Similar overlapped spectra to that of Fig. 3(b) could be easily found from commercial available cells like Rb cell #1 and previous papers [17,18]. Spectra in Fig. 3 were fitted by the Lorentzian-transit time function [19], from which we derived the transit time broadening (FWHM) of 162 kHz and the natural linewidth of 346 kHz, which agrees with the value estimated in Ref. [18] (300 kHz). We thus update the clock frequencies via Rb cell #3, listed in Table 1 with the error budget described in Table 2. The statistic error in Table 2 is derived from the standard deviation of the spectra repeatability test (nine scans); the light shift error comes from the fitting uncertainty in Fig. 4(c); the collision shift and the error of extrapolation to 90°C saturation vapor pressure are estimated from the data of –27 ± 2 Hz/μTorr reported in Ref. [16] and from the maximum value of 5.3 ± 2 μTorr monitored by our vacuum gauge (see Fig. 1(c)); the Zeeman shift is negligible under the environment of smaller than 1 mG magnetic field, according to the result of Refs. [1,4]. Since the reported Rb clocks were all working among 90 to 100°C cell temperature [17], we extrapolating

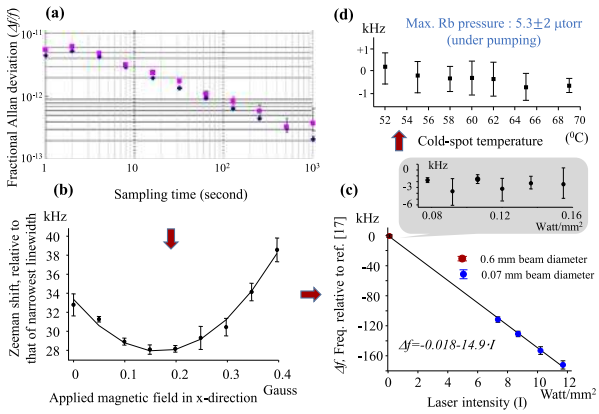

Fig. 4. SOP for self-calibrating ω_c (see text for details). The red dot in (c) is an average of the gray-inset data.

our result to 90°C according to Ref. [16]. The obtained clock frequency via Rb cell #3 agrees with that recommended by CIPM (Comité international des poids et mesures, [14]) within the quoted errors. On the other hand, most of the frequencies obtained via Rb cell #2 in Table 1 always yielded redshifts of around 28 kHz to Rb cell #3. We suspect that the 28-kHz shift of Rb cell #2 resulted from some collision partners like He and N_2 [16]. In particular, the Rb cell wall #2 was constantly heated up to 90°C, which enhanced both the N_2 outgassing from the cell wall and the He permeation from the atmosphere [8].

A standard operation procedure (SOP) illustrated in Fig. 4 is proposed for self-calibrating the ω_c. First, keep the laser instability better than its inaccuracy at an integration time similar to the data acquisition time needed to sketch out the entire transition. It takes 900 s to resolve the clock transition, and the red dots in Fig. 4(a) show that the Allan deviation reaches 3.1×10^{-13} at 1000 s, which is much smaller than the frequency inaccuracy (±2.4 kHz, 1σ) quoted in Table 1. The red dots in Fig. 4(a) were derived from the beat note between our Rb_{opt} clock and one cesium clock-based [20] Ti:S comb laser, while the blue dots were from the beat note between two independent cesium clocks [20]. The comparison in Fig. 4(a) implies that the instability of our Rb-stabilized laser is qualified to be a clock. Second, observe the Zeeman shift in the most sensitive direction (x direction) to confirm if the turning point in Fig. 4(b) is consistent with the minimum linewidth in Fig. 2(b). We found that the approach of "linewidth measurement" is more sensitive than that of the "frequency shift measurement" in our scheme. Third, make sure that the laser frequency would not be changed within our measurement precision, even the laser power and cold-spot temperature were varied to a wide range as illustrated in the gray inset of Fig. 4(c) and in Fig. 4(d). The red dot in Fig. 4(c) represents the average power of the gray inset (power meter not calibrated). The laser frequency was found to be near that at zero intensity and zero Rb–Rb effective collision [16], within the aforementioned 2.4-kHz precision. This could be verified by comparing with the extrapolating result of the light shift in Fig. 4(c) and the pure Rb-Rb effective collision shift measured in Ref. [16] (–27 ± 2 Hz/μTorr). Note that the existence of alien gas commented previously on Rb cell #2 will lead to a different collision shift at a BIPM-recommended temperature (below 100°C) [14]. We thus suggest that the frequency standard be redefined at zero intensity and at the Rb pressure below 5 ± 5 μTorr, where the spectral

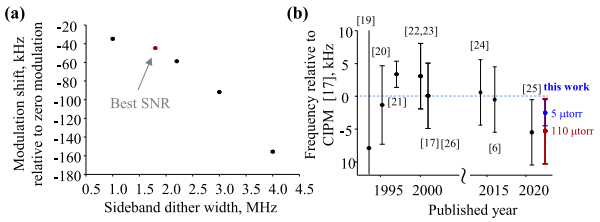

Fig. 5. (a) Modulation (dither) shift, measured via Rb cell #1; red dot, the dither width used in this paper. (b) Comparisons with previous experiments. Blue dot, 5 μTorr Rb pressure; red dot, extrapolating to 110 μTorr (90°C Rb saturation pressure).

linewidth of clock transition is below 510 kHz and then the frequency is 385285142372.0 (2.4, 1σ) kHz. An extrapolation to 110 ± 5 μTorr (90°C saturation vapor pressure) is performed for comparing with previous experiments displayed in Fig. 5, which leads to the frequency in Table 1 as 385285142374.8 (5.0, 2 σ). This value is very near what was measured recently from NIST [17].

In conclusion, our scheme avoids two systematic errors and reduces the stray magnetic field inside the Rb container to a negligible level; hence we give an updated clock frequency and offer an unmodulated carrier frequency ω_c for users. Here we want to emphasize, with Fig. 5(a), that the "modulation shift" is easy to appear practically [10] when the laser frequency was widely dithered for high SNR. Therefore, the stabilized ω_c needs to be self-calibrated occasionally in case a frequency shift happens to the Rb cell #1 system, which might be owing to the change of the dither width or the glass cell contamination from either atmospheric helium [8] or cell wall outgassing, since the Rb cell #1 is heated up to 90°C. After each calibration, the EOM1 frequency (Δ_0) adjusted to meet the spectral line center of clock transition is then recorded and used to keep ω_c always equaling to the determined frequency of 385285142372.0 (2.4. 1σ) kHz, without the need to worry about the aforementioned frequency shifts in the Rb cell #1 system. Fig. 5(b) demonstrates the comparisons with previous results [6,14,17,18,21–26].

Funding. National Science and Technology Council (111-2112-M-008-027).

Acknowledgment. We thank Drs. Chi Lee, Jia-Wei Chang, and Hsin-Hung Yu for helping us for the systematic studies.

Disclosures. The authors declare no conflicts of interest

Data availability. Data underlying the results presented in this paper are not publicly available at this time but may be obtained from the authors upon reasonable request.

REFERENCES AND NOTES

1. N. D. Lemke, K. W. Martin, R. Beard, *et al.*, Sensors **22**, 1982 (2022).
2. W.-Y. Cheng, T.-J. Chen, C.-W. Lin, *et al.*, Opt. Express **25**, 2752 (2017).
3. M. Lezius, T. Wilken, C. Deutsch, *et al.*, Optica **3**, 1381 (2016).
4. D. K. W. Martin, G. Phelps, N. D. Lemke, *et al.*, Phys. Rev. Appl. **9**, 014019 (2018).
5. V. Maurice, Z. L. Newman, S. Dickerson, *et al.*, Opt. Express **28**, 24708 (2020).
6. O. Terra and H. Hussein, Appl. Phys. B **122**, 27 (2016).
7. T.-W. Liu, B.-W. Chen, H.-H. Yu, *et al.*, Opt. Lett. **48**, 2421 (2023).
8. K–H Chen, C.-M. Wu, S.-R. Wu, *et al.*, Opt. Lett. **45**, 4088 (2020).
9. M. Nakazawa, J. Appl. Phys. **59**, 2297 (1986).
10. C.-M. Wu, T.-W. Liu, and W.-Y. Cheng, Phys. Rev. A **92**, 042504 (2015).
11. Optromix Inc., Model Number SFY-1080-01000-L-FA, https://optromix.com/.
12. J. M. Khosroflan and B. A. Garetz, Appl. Opt. **22**, 3406 (1983).
13. C.-M. Wu, T.-W. Liu, M.-H. Wu, *et al.*, Opt. Lett. **38**, 3186 (2013).
14. T. J. Quinn, Metrologia **40**, 103 (2003).
15. N. Allard and J. Kielkopf, Rev. Mod. Phys. **54**, 1103 (1982).
16. N. D. Zameroski, G. D. Hager, C. J. Erickson, *et al.*, J. Phys. B **47**, 225205 (2014).
17. Z. L. Newman, V. Maurice, C. Fredrick, *et al.*, Opt. Lett. **46**, 4702 (2021).
18. C. S. Edwards, G. P. Barwood, H. S. Margolis, *et al.*, Metrologia **42**, 464 (2005).
19. F. Biraben, M. Bassini, and B. Cagnac, J. Phys. France **40**, 445 (1979).
20. Symmetricom 5071a cesium clock, whose frequency was traced to UTC (Coordinated Universal Time) via the flying clock method, resulted in 1.4×10^{-14} one-day accuracy and 10^{-11} for 10 second sampling time.
21. F. Nez, F. Biraben, R. Felder, *et al.*, Opt. Commun. **102**, 432 (1993).
22. R. Felder, D. Touahri, O. Acef, *et al.*, SPIE Proceeding **2378**, 52 (1995).
23. D. Touahri, O. Acef, A. Clairon, *et al.*, Opt. Commun. **133**, 471 (1997).
24. S. A. Diddams, D. J. Jones, L.-S. Ma, *et al.*, Opt. Lett. **25**, 186 (2000).
25. D. J. Jones, S. A. Diddams, J. K. Ranka, *et al.*, Science **288**, 635 (2000).
26. P. V. K. Kumar and M. V. Suryanarayana, Pramana - J Phys **83**, 189 (2014).